Solid State Science and Technology, Vol. 23, No 1 & 2 (2015) 99-107
ISSN 0128-7389 | *http://journal.masshp.net*

STRUCTURE, MICROSTRUCTURE AND MAGNETIC PROPERTIES STUDY OF CERAMIC COMPOSITE $(La_{0.67}Ca_{0.33}MnO_3)_{1-x}/(\text{Nano-sized}\alpha\text{-}Fe_2O_3)_x$

W. N. W. Wan Jusoh, K. P. Lim, M. M. Awang Kechik,
S. A. Halim and S. W. Ng

Superconductor Laboratory, Department of Physics, Faculty of Science, Universiti Putra Malaysia, 43400 Serdang, Selangor.

Corresponding author: limkp@upm.edu.my

ABSTRACT

The structural, microstructure and magnetic properties of polycrystalline $(La_{0.67}Ca_{0.33}MnO_3)_{1-x}/(\alpha\text{-}Fe_2O_3)_x$ composites where x = 0%, 5%, 10%, 15%, 20% were investigated. Polycrystalline $La_{0.67}Ca_{0.33}MnO_3$ (LCMO) was synthesized via solid state reaction at high sintering temperature while for nano-sized Fe_2O_3 (20-50 nm) a commercial product was used. X-ray diffraction (XRD) patterns show that parent compound of $La_{0.67}Ca_{0.33}MnO_3$ is a single phase without any detectable impurity and give orthorhombic structure with space group *Pbnm* (62) while $\alpha\text{-}Fe_2O_3$ is in cubic form with space group I a -3 (206). As Fe_2O_3 content x increases, the magnetization M values decrease as observed via Vibrating Sample Magnetometer (VSM) at room temperature. Higher magnetization is noticed inpure LCMO rather than in LCMO composites added with $\alpha\text{-}Fe_2O_3$. However, Scanning Electron Microscopy (SEM) shows that nano-sized Fe_2O_3 mainly distributed at the grain boundary of $La_{0.67}Ca_{0.33}MnO_3$. The particle size of LCMO composites shows fluctuation; meanwhile particle size of $\alpha\text{-}Fe_2O_3$ shows almost similar values except for sample with the addition of 15% of $\alpha\text{-}Fe_2O_3$ where lowest particle size with higher coercivity and retentivity are observed. As compared to pure $La_{0.67}Ca_{0.33}MnO_3$, Fe_2O_3 doping level at the grain boundaries can be assumed to modify the magnetic properties of $La_{0.67}Ca_{0.33}MnO_3$.

Keywords: Bulks; structura; grain boundaries; magnetic materials; perovskite manganites;

INTRODUCTION

The discovery of colossol magnetoresistance (CMR) in the perovskite manganites $RE_{1-x}AE_xMnO_3$ where (RE = La, Pr, Nd and AE = Sr, Ca, Ba, Pb) have been a popular subject due to its unusual electrical and magnetic properties [1]. Much effort has been devoted to achieve improved LFMR of perovskite manganites by forming manganite composites with fillers such as a magnetic material (Ni-ferrite, Fe_2O_3, etc.) [2,3], an insulator (CeO_2, $SrTiO_3$, Al_2O_3, SiO_2, etc.) [4,5,6], metallic oxide (ZnO, CuO, Ag_2O, etc.) [7,8] and even other manganite ($LaMnO_3$, etc.). As known, there are two types of CMR effects that have been found in these manganites, namely is the intrinsic CMR

and extrinsic CMR. The intrinsic CMR is caused by double exchange mechanism proposed by Zener in 1951 [9] which is useful to explain the phenomena of CMR observed near the Curie temperature (T_c) at a relatively high magnetic field (up to 10 kOe). Meanwhile, the extrinsic CMR is strongly related to the grain boundaries, artificial grains boundaries and atomic defects in the film-substrate interface[5,7]. Spin-polarised tunneling or spin dependent scattering among neighboring grains took a responsibility in order to explain this kind of CMR effect. Therefore, this extrinsic effect may enhance low-field magnetoresistance (LFMR) in wide range temperature range, thus can be useful in sensor application.

The magnetic behavior in this manganite is well proven to be sensitive at the doping on Mn sites. The most nearest neighbors of Mn in the periodic table is Fe element and its radius is close to Mn. Furthermore, Fe is able to substitute either Mn^{3+} or Mn^{4+} ion as Fe and Mn have similar energy level structure and both have multiple valences [10]. Therefore, doping Fe on the Mn site is expected to have useful information in view to the understanding of the mechanism in these systems. The magnetotransport property in these compounds can be explained by double exchange (DE) mechanism that consider the magnetic coupling between Mn^{3+} and Mn^{4+}. However, double exchange mechanism alone cannot explain the colossal magnetoresistance (CMR) and other phenomena observed in these manganite compounds. An interesting proposal is that the carriers phase separation is an essential ingredient to the understanding of the CMR materials.
In this article, the influence of Fe doping on the structure, microstructure and magnetic properties for hole doped $(La_{0.67}Ca_{0.33}MnO_3)_{1-x}/(\alpha\text{-}Fe_2O_3)_x$ composite are mainly discussed. The bulk polycrystalline sample of $La_{0.67}Ca_{0.33}MnO_3$ (LCMO) was prepared successfully via solid state technique. Pre-sintered powder was added with different weight percentage (5%, 10%, 15%, 20%) of Fe_3O_4 nanopowders of 20-50 nm in size.

MATERIALS AND METHOD

The polycrystalline samples were synthesized by solid state reaction method. LCMO was prepared by mixing Lanthanum(III) Oxide, 99.9%, Calcium Carbonate, 99.95%, Manganese(IV) oxide, 99.9% in stoichiometric proportions with high ball-milling for 24 hours and dried in the oven at 100°Cfor 6 hours. The homogeneous powder was ground and calcined at 900°C for 12 hours and reground for 1 hour before pre-sintered in an open tube furnace at 1200°C in 24 hours. The obtained pure $La_{0.67}Ca_{0.33}MnO_3$ powder and Fe_2O_3-α powder (20-50 nm) with 98% purity were well mixed. The samples of nominal $(La_{0.67}Ca_{0.33}MnO_3)_{1-x}/(\alpha\text{-}Fe_2O_3)_x$with x = 0%, 5%, 10%, 15% and 20% were pressed and annealed at 800°C in 2 hours. The structural and microstructure of the samples were characterized by X-ray diffraction(XRD, Phillips PW 3040/60 Xpert Pro) using a CuKαradiation at room temperature and scanningelectron microscopy (SEM, LEO1455 VSPEM, with an OXFORD INCA ENERGY 300EDXattachment). The ferromagnetic-paramagnetic (FM-PM) behaviors were measured by vibrating sample magnetometer (VSM) at room temperature.

RESULTS AND DISCUSSIONS

.

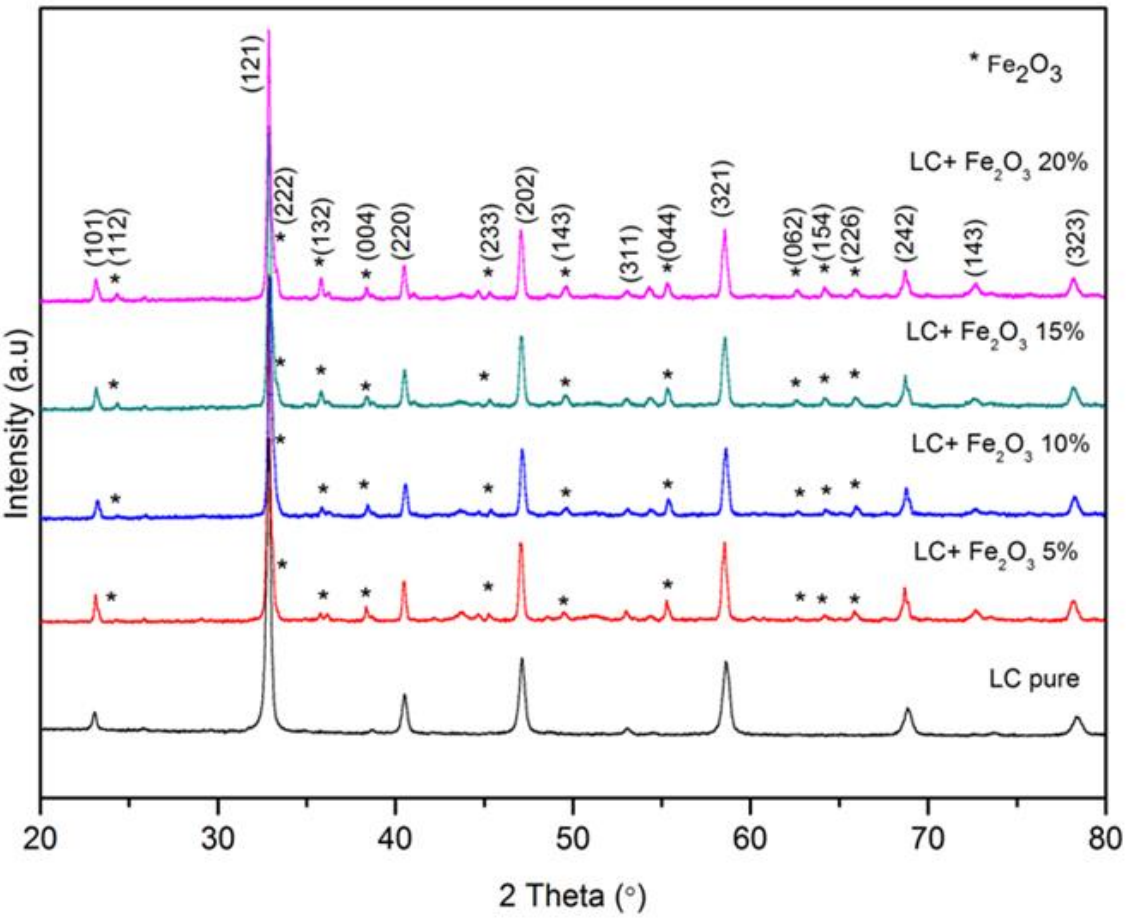

Figure 1: XRD spectrum of $La_{0.67}Ca_{0.33}MnO_3$ of pure, 5%, 10%, 15% and 20%

Table 1:Rietveld Refinement of $La_{0.67}Ca_{0.33}MnO_3$ of pure, 5%, 10%, 15% and 20%

Sample code	LCMO				
Sample	$La_{0.67}Ca_{0.33}MnO_3$				
Structure type	Orthorhombic				
Space group	P n m a (62)				
Composition Fe_2O_3	0%	5%	10%	15%	20%
LCMO ICSD sample	56661				
a /Å	5.4567(1)	5.4695(4)	5.4697(5)	5.4703(5)	5.4688(6)
b /Å	7.7118(2)	7.7310(5)	7.7313(6)	7.7322(6)	7.7315(7)
c /Å	5.4729(1)	5.4872(3)	5.4874(4)	5.4877(4)	5.4877(5)
Volume /$Å^3$	230.30480	232.02680	232.04800	232.11850	232.03380
Density g/ cm^3	6.0249	5.9887	5.9881	5.9863	5.9885
∠Mn-O(1)-Mn (°)	160.179	162.572	162.572	162.572	162.571
∠Mn-O(2)-Mn(°)	160.860	161.157	161.157	161.158	161.157
Mn-O(1) (Å)	1.960 x4	1.937 x2 1.982 x2	1.937 x2 1.982 x2	1.937 x2 1.982 x2	1.937 x2 1.982 x2
Mn-O(2) (Å)	1.955 x2	1.959 x2	1.959 x2	1.959 x2	1.959 x2
Sample code	-	Fe_2O_3			
Fe_2O_3 ICSD Sample	-	108905			
Structure type	-	Cubic			
Space group	-	I a -3 (206)			
a /Å	-	9.4157(6)	9.4158(7)	9.4157(8)	9.413(1)
b /Å	-	9.4157(6)	9.4158(7)	9.4157(8)	9.413(1)
c /Å	-	9.4157(6)	9.4158(7)	9.4157(8)	9.413(1)
Volume /$Å^3$	-	834.74230	834.79130	834.75240	833.91600
Density g/cm^3	-	5.0820	5.0817	5.0820	5.0871
R_P (%)	4.24316	4.12562	3.70370	3.81069	3.89208
R_{WP} (%)	5.92030	5.90074	5.13811	5.58562	6.17936
R_{EXP} (%)	3.91532	2.99905	3.07959	2.79730	2.66277
Goodness of fit (S)	2.28640	3.87121	2.78369	3.98718	5.38542

The crystal structure for all samples were studied with X-ray diffraction (XRD) at room temperature as shown in Figure 1. The XRD pattern of $(La_{0.67}Ca_{0.33}MnO_3)_{1-x}$ $(Fe_2O_3-\alpha)_x$ showed some changes with the addition Fe_2O_3 (x=5%, 10%, 15%, 20%). For pure $La_{0.67}Ca_{0.33}MnO_3$ sample, only a typical perovskite structure with single phase and no

detectable impurity phases are observed. XRD patterns corresponding to LCMO phase in the sample at room temperature is matched with the standard $La_{0.67}Ca_{0.33}MnO_3$ (ICSD collection code: 56661) with structural orthorhombic and space group *Pnma* (62). While,XRD analysis for all composite samples show true set of XRD spectrum corresponding to LCMO and α-Fe_2O_3 phase is matched with the standard α-Fe_2O_3 (ICSD collection code:108905) with space group I a -3 (206) and structure of cubic. Detailed studied for interatomic distance and bond angle of MnO_6 for all samples has been carried out as shown in the Table 1 and we noticed that the changes of lattice constants in our samples are not obvious. This shows that the α-Fe_2O_3 formed did not diffuse inside the LCMO systems and it stay outside the LCMO phase. If there is replacement of Mn ions by Fe ions, it does not influence too much on its lattice parameters due to the closeness of the ionic sizes and low Fe doping [10]. Thus, the volume of LCMO and α-Fe_2O_3 is about the same since lattice parameter is almost similar for all samples. Therefore, the interatomic distance and bond angle for all samples is significant which means addition of iron oxide nanopowder does not affect the shape and structure of pure LCMO.

Figure 2 (a) shows the microstructures of pure $La_{0.67}Ca_{0.33}MnO_3$ and $La_{0.67}Ca_{0.33}MnO_3$/ α-Fe_2O_3 (x = 5%, 10%, 15%, 20%). All figures show clear grain boundaries. In addition, the chemical homogeneity of pure LCMO and α-Fe_2O_3 doped samples was measured by energy dispersive X-ray analysis (EDX) as shown in Figure 2(b). For this purpose, La:Ca:Mn ratio and Fe distribution in different positions within a separate grain was analysed. EDX spectra of the doped composite shows Fe_2O_3 peak along with La, Ca, Mn and O peaks, which also support the presence of Fe_2O_3 in the doped composite. By increasing the percentage of Fe_2O_3 the microstructure of the composite is apparently changed, where a lot of small grains are detectable. From the core to the surface of the grain, the content of Fe_2O_3enhances. This means even though Fe_2O_3 may dissolve in the LCMO lattice, it can also exist outside the grain. The reasons for these diverse distributions can be interpreted from the relation of lattice strain because the radius of Fe^{2+} ions (0.78 Å) is larger than Mn^{3+} ions (0.65 Å) and Mn^{4+} ions (0.53 Å), larger ions in the lattice might be pushed out towards the grain boundaries in order to release local strain [7]. Therefore, Fe_2O_3exists outside the grain and grain boundaries of LCMO. From Table 2, the average particle size of α-Fe_2O_3 and LCMO was listed with increases of the percentage of α-Fe_2O_3.The fluctuating average particles size of LCMO as shown in Figure 3 where it is decreasing at 5% and started to increase at 10% and the biggest grain size of LCMO at 20% doped is noticed. However, the α-Fe_2O_3 particles size shows small changes of dropping with the percentage of Fe_2O_3 addition and smallest particle size is observed in 15% doped sample. Overall, each sample shows different grain size which it contribute to different diffusion rate during sintering process. Rate of diffusion is also influenced by the physical size of each starting compound and distribution rate.

Table 2: Average particles size of α-Fe_2O_3 and LCMO

Percentage of α-Fe_2O_3 (%)	Average particles size α-Fe_2O_3 (nm)	Average particles size LCMO (μm)
0	-	1.52
5	130	1.33
10	100	1.97
15	76	1.80
20	110	2.19

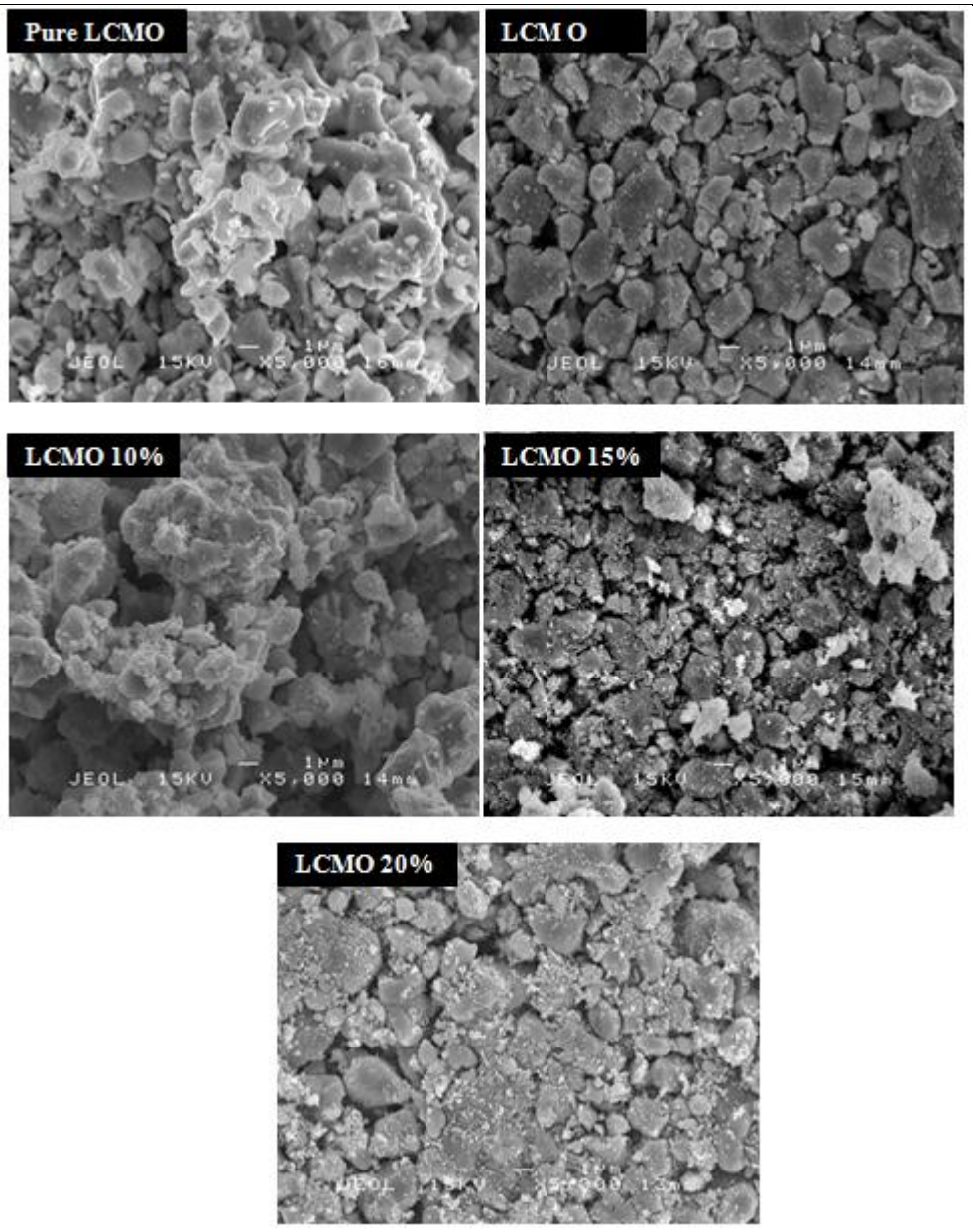

Figure 2 (a): SEM images of $La_{0.67}Ca_{0.33}MnO_3$ / Fe_2O_3 with x = 0%, 5%, 10%, 15%, 20%

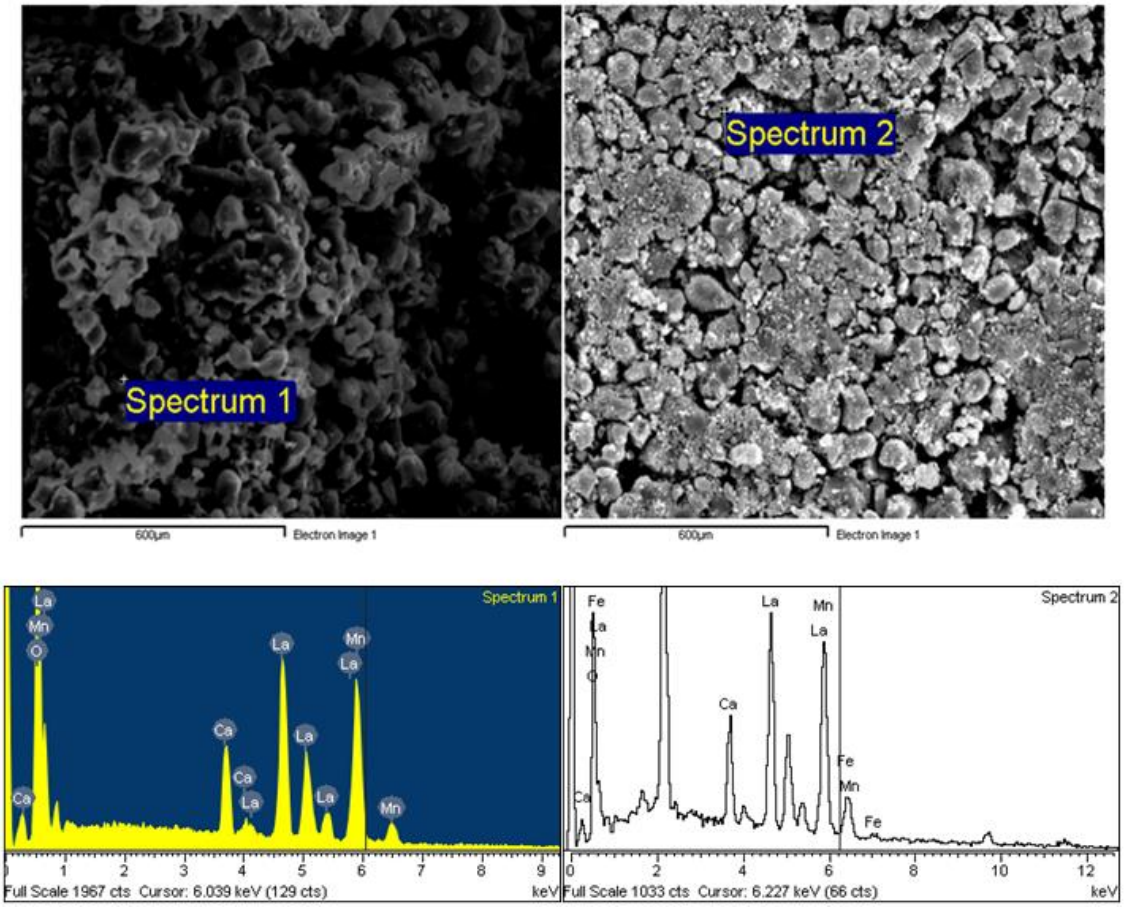

Figure 2 (b): EDX patterns of pure LCMO [left] and x = 20% distribution of Fe_2O_3 [right]

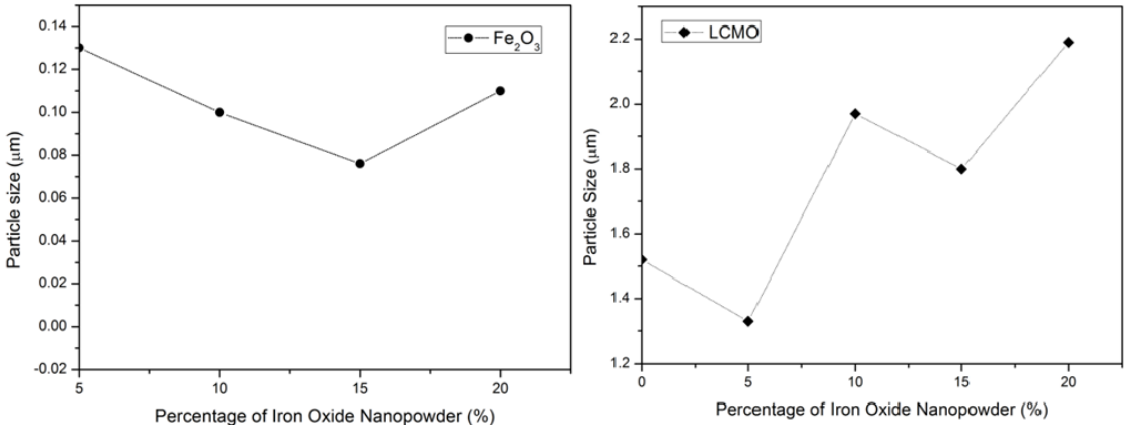

Figure 3: Particle size distribution of LCMO and α-Fe_2O_3

Figure 4 shows the magnetization versus magnetic field for LCMO/α-Fe_2O_3 composite samples at room temperature. As observed, the magnetization decreases as the percentage of α-Fe_2O_3 increases and pure LCMO has highest magnetization rather than the composites. Table 3 indicates that the magnetization decreases with the increase of α-Fe_2O_3 percentages. However, the coercivity and retentivity values do not show conclusive trend due to the fluctuation of the values. From SEM result, the particle size drop to about 76 nm at 15% α-Fe_2O_3, this might be due to the maximum coercivity of α-Fe_2O_3 composite occurs within its single domain range and to change the magnetization of a single domain grain is to rotate the magnetization, thus an energetically difficult process resulting single domain magnetically hard and have high coercivity and remanence. However, for a larger and smaller grain size, the coercivity decreases. The larger grain size is due to the grain subdivides into domains and for the smaller grain size is due to the randomizing effects of thermal energy. Overall, weak antiferromagnetic of α-Fe_2O_3 phase accompany with paramagnetic of LCMO phase is observed at room temperature for all samples and the antiferromagnetic is weaken as α-Fe_2O_3 phase increases.

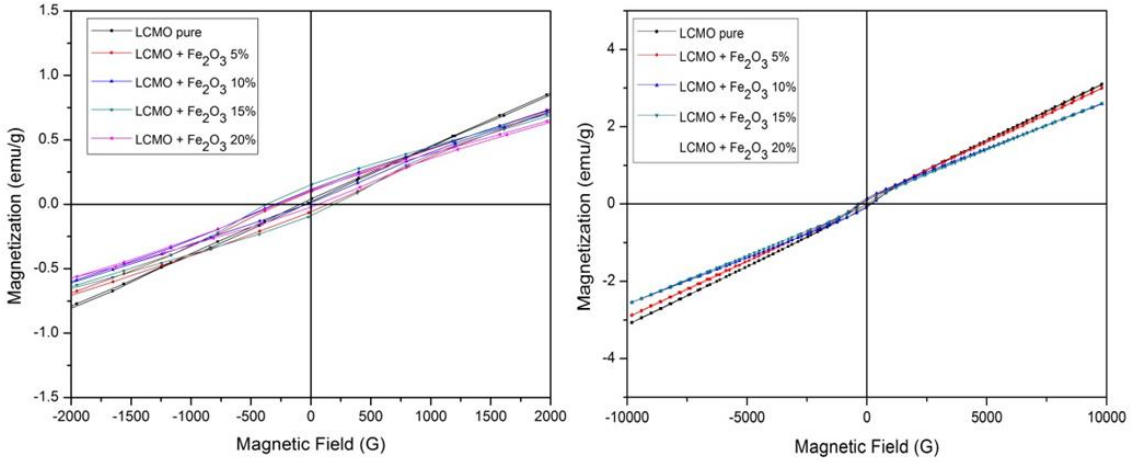

Figure 4:Magnetization versus magnetic field of LCMO with Fe_2O_3 nanopowder

Table 3: Magnetization, Coercivity and Retentivity of LCMO sample with different % α-Fe_2O_3

Percentage of Fe_2O_3 (%)	Magnetization (emu/g)	Coercivity (G)	Retentivity (emu/g)
0	4.0512	23.956	0.011321
5	3.0883	198.67	0.078819
10	2.9429	133.82	0.051466
15	2.6830	262.55	0.14829
20	2.5749	170.28	0.055302

CONCLUSION

In this work, $La_{0.67}Ca_{0.33}MnO_3$ had been successfully fabricated using standard solid state reaction method where α-Fe_2O_3 nanopowder is used as fillers to form $La_{0.67}Ca_{0.33}MnO_3$-nanosized α-Fe_2O_3 composite.XRD analysis shows that $La_{0.67}Ca_{0.33}MnO_3$-nanosized Fe_2O_3 obtained peak were matched with the standards $La_{0.67}Ca_{0.33}MnO_3$ spectrum (ICSD collection code:56661). From rietveld refinement, the interatomic distance and bond angle for all samples do not undergo changes and almost similar indicating that addition of iron oxide nanopowder does not affect the shape and structure of pure LCMO. Analysis of microstructure of sample using SEM shows the fluctuation of average particles size of LCMO. However, the α-Fe_2O_3 particles size is almost similar except for 15% doped as its grain size in single domain range which is much smaller than others thus resulting in high coercivity and retentivity. Magnetization of the composites decrease with increasing percentage of α-Fe_2O_3. Pure LCMO sample displayed paramagnetic behavior at room temperature and with the addition of α-Fe_2O_3 a combination of paramagnetic and antiferromagnetic behaviors were observed.

ACKNOWLEDGEMENTS

The authors gratefully acknowledge the support from the Ministry of Education (MOE) forthe grant under the Fundamental Research Grant Scheme (FRGS) vote: 02-01-14-1469FR: Enhancement of Magnetoresistance Effect in La-(Sr, Ca)-Mn-O/Sb_2O_3, CeO_2, Al_2O_3 Composites for Low-Field Magnetic Sensor.

REFERENCES

[1]. Z.-Q. Xue, D. Ming-Xing, W. Ren-hui, F. Xin-Nan, W. Yang, Xia Zheng-Cai, *Chinese Phys. Lett.* 2194 (23AD) 2194.
[2]. B.B. Nayak, S. Vitta, D. Bahadur, *Mater. Sci. Eng. B.* **139** 171–176 (2007)
[3]. A. Marzouki-Ajmi, W. Cheikrouhou-Koubaa, A. Cheikhrouhou, *J. Supercond. Nov. Magn.* **28** 103–108 (2015)
[4]. H. Liu, Y. Luo, M. Li, *J. Mater. Process. Technol.* **202** 347–352 (2008)
[5]. D. Bahadur, D. Das, *J. Chem. Sci*. **115** 587–606 (2003)
[6]. D. Das, P. Chowdhury, R.N. Das, C.M. Srivastava, A.K. Nigam, Solution sol – gel processing and investigation of percolation, 3 (n.d.).
[7]. L.W. Lei, Z.Y. Fu, J.Y. Zhang, H. Wang, *Mater. Sci. Eng. B.* **128** 70–74 (2006)
[8]. L.W. Lei, Z.Y. Fu, J.Y. Zhang, H. Wang, *Solid State Commun.* **140** 261–266 (2006)
[9]. C. Zener, *Phys. Rev.* **82** 403–405 (1951)
[10]. T.P. Lu, C.C. Wu, M.D. Lan, *Phys. B Condens. Matter.* **405** 2891–2895 (2010)